The motional Stark effect diagnostic on NSTX[a)]

F. M. Levinton and H. Yuh
Nova Photonics, Inc., Princeton, New Jersey 08540, USA

(Received 15 May 2008Received 11 May 2008; accepted 14 July 2008; published online 31 October 2008)

This work describes the implementation and recent results from the motional Stark effect (MSE) collisionally induced fluorescence diagnostic on NSTX. Due to the low magnetic field on NSTX the MSE diagnostic requires a new approach for the viewing optics and spectral filter. This has been accomplished with a novel optical design that reduces the geometric Doppler broadening, and a high throughput, high resolution spectral filter to optimize signal-to-noise ratio. With these improvements the polarization fraction is ~30%–40% and, combined with the large throughput, a time resolution of ~5 ms. The MSE diagnostic presently has 16 sight lines operating, providing measurements of the magnetic field line pitch from the plasma center to near the outboard edge of the plasma. © *2008 American Institute of Physics.* [DOI: 10.1063/1.2968699]

I. INTRODUCTION

Over the past several years the motional Stark effect (MSE) diagnostic[1] has become established as the standard technique for determining the q profile in tokamaks. The worldwide adoption of MSE polarimetry is due to its very good temporal and spatial resolutions, combined with its exceedingly good accuracy. This has resulted in many important scientific contributions toward the understanding of stability[2–6] and transport[7–9] and has had a significant impact on the fusion program.

The NSTX experiment is a low-aspect-ratio spherical torus[10,11] that operates at a toroidal magnetic field of 0.30–0.55 T. This is a significantly lower toroidal magnetic field than any previous implementation of MSE diagnostic based on collisionally induced fluorescence (MSE-CIF) has operated at. The spectral shift of the Stark multiplet is linearly proportional to the magnetic field and at low magnetic field causes overlap of the Stark multiplet transitions due to the finite linewidth from beam divergence and geometric Doppler broadening. This makes implementation of MSE much more challenging. We have extended the lower limit of the operating range of the diagnostic down to 0.30 T with a new design of the collecting optics to minimize the spectral broadening from geometric effects, and with the development of a narrow bandpass spectral filter with a wide field of view.

II. MOTIONAL STARK EFFECT POLARIMETRY DIAGNOSTIC

The principle of the measurement relies on the Stark effect[12] from the Lorentz electric field, $\vec{\mathbf{E}}=\vec{\mathbf{v}}\times\vec{\mathbf{B}}$, as an energetic neutral beam propagates across a magnetic field. Polarimetry measurements[13,14] of the direction of the linearly polarized π or σ component emission results in a measure of the magnetic field pitch angle, $\gamma_p=\tan^{-1}(B_p/B_T)$, where B_p is the poloidal magnetic field and B_T is the toroidal magnetic field. The polarization fraction is defined as $P_f=(I_\parallel-I_\perp)/(I_\parallel+I_\perp)$, where P_f is the polarization fraction and $I_{\parallel,\perp}$ is the intensity of light polarized parallel or perpendicular to the magnetic field. The polarization fraction is an important parameter for the MSE diagnostic, as the signal-to-noise ratio is proportional to it. At high magnetic field there is a large Stark shift relative to the width of the spectral transitions. This makes it relatively easy to separate out the σ and π transitions with an interference filter and obtain a high polarization fraction. At lower magnetic fields the Stark shift can be less than the spectral linewidth, resulting in overlap between the two polarization intensities and a poor polarization fraction. In general, for a MSE measurement the Stark shift should be greater than the spectral linewidth to get a sufficiently high polarization fraction.

For an MSE diagnostic based on collisionally induced fluorescence (MSE-CIF) the spectral linewidth is subject to two sources of line broadening. The first is from the finite beam divergence, producing Doppler broadening of the line. The beam divergence is a combined effect from the ion thermal temperature in the source and the ion optics used for the beam extraction. In our model we use a divergence that was previously measured.[15] The other source arises from geometrical effects: spectral broadening from the finite size of the collection lens and the finite object size of the beam imaged onto the detector. For a finite size lens, a point that is imaged from the beam will have different crossing angles through the lens, and hence a different Doppler shift. The larger the lens size, the larger is the range of crossing angles from the beam, and the broader is the spectral width. A similar effect occurs for a finite size of beam imaged by the lens. A substantial improvement can be obtained by recognizing that the geometric Doppler broadening comes from the horizontal angular variation at the lens (parallel to the beam direction) and very little Doppler broadening occurs from the

[a)]Contributed paper, published as part of the Proceedings of the 17th Topical Conference on High-Temperature Plasma Diagnostics, Albuquerque, New Mexico, May 2008.

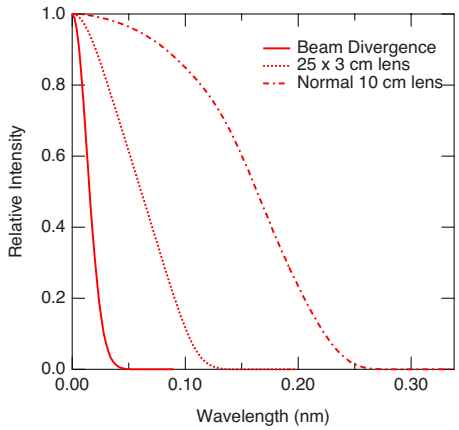

FIG. 1. (Color online) Computed spectral broadening, relative to the Doppler shifted line center, from beam divergence (solid line), masked lens (dot), and regular lens (dash-dot line).

vertical variation (perpendicular to the beam direction). By aperturing the lens such that the collecting area is masked horizontally the geometric Doppler broadening is reduced. Shown in Fig. 1 is a comparison of a 25 cm diameter lens with a 3 cm aperture and a 10 cm diameter lens without any aperture. The computed spectral linewidth [full width at half maximum (FWHM)] for a 0.3 T magnetic field, including beam divergence and geometrical broadening, is ~0.3 nm. This compares to a Stark shift of only 0.05 nm. The convolution with the Stark multiplet, with a 0.075 nm wide filter and a nonapertured 10 cm lens, results in a polarization fraction of only 3%, as shown in Fig. 2. This compares to a Stark shift of 0.7 nm and a polarization fraction of ~75% at 4 T. A 3% polarization fraction is much too low to make a MSE measurement, since this reduces the signal-to-noise ratio by a factor of 25. This would require increasing the light throughput by a factor of 625, ($S/N \propto \sqrt{I}$), to maintain the same measurement uncertainty. Shown in Fig. 3 is a measured spectrum from NSTX of the Doppler shifted H_α emission from

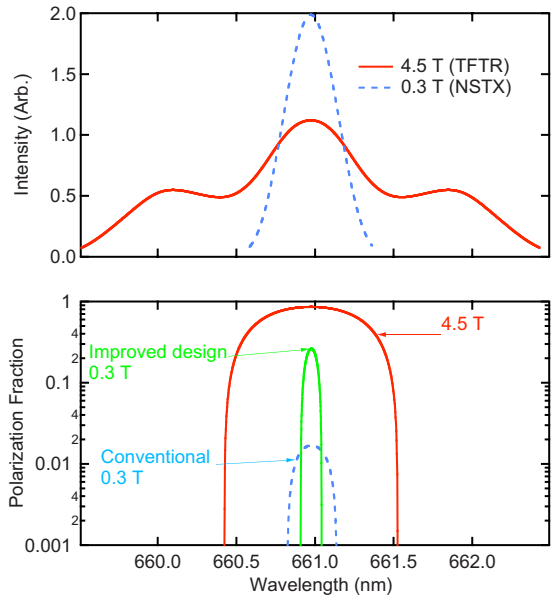

FIG. 2. (Color online) The computed intensity profiles (upper panel) and polarization fraction profile (lower panel) at 4.5 and 0.3 T.

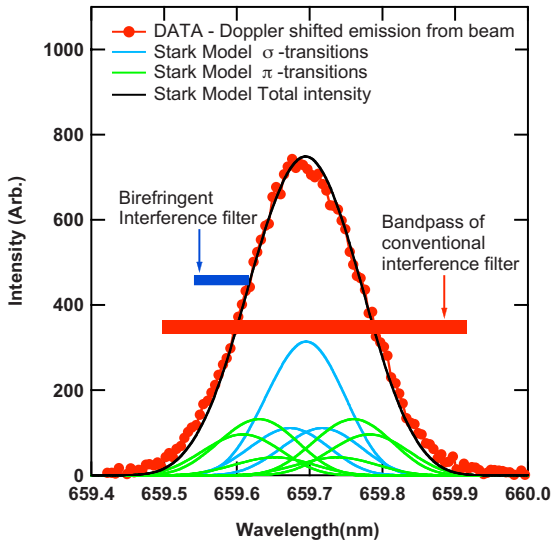

FIG. 3. (Color online) Measured spectrum from NSTX of Doppler shifter H_α emission from the heating beam. Comparison of the calculated Stark multiplet and its convolution is compared to the measured spectra.

the heating beam. For comparison is the calculated Stark multiplet and its convolution compared to the measured spectra. A conventional interference filter with a bandpass of 0.3–0.4 nm would integrate over the entire Stark multiplet of π and σ transitions. The narrow band Lyot filter can isolate a portion of the spectra, such as the π lines, to yield a much higher polarization fraction, measured to be 40%.

A numerical model was developed to vary the lens aperture and filter passband in order to optimize the signal-to-noise ratio. Both parameters were varied, independently, and the signal throughput and polarization fraction were calculated using the computed linewidth. The lens aperture width and filter bandwidth that gave the optimal signal-to-noise ratio are 3 cm and 0.060 nm, respectively. With this lens aperture and filter passband, the polarization fraction is 30%–40%, which makes the MSE-CIF technique quite feasible. With a higher throughput optical system and improved detector quantum efficiency the signal-to-noise ratio is comparable to MSE systems on high field devices.

III. BIREFRINGENT OPTICAL FILTER

In order to realize the advantage of this technique, a very narrow passband, high throughput spectral filter, ~0.06 nm FWHM, is required. This is beyond the current technology for interference filters which can go down to 0.1 nm FWHM for dual cavity and 0.3 nm FWHM for triple cavity. Fabry–Pérot interferometers have the required resolution but do not have sufficient acceptance angle to match the étendue of the collection optics without going to a very large diameter. Wide field birefringent filter,[16] such as the modified Lyot[16] filter and wide field Michelson interferometer[17] have been fabricated with spectral resolutions as low as 0.01 nm and an angular acceptance almost an order of magnitude larger than a Fabry–Pérot.[18]

We have designed and built a wide field Lyot filter. The principle of operation of the filter is based on interference of light created by a phase delay in a birefringent crystal. In the

Lyot filter, light entering the filter is split by a linear polarizer into two equal parts, along the fast and slow axis of a birefringent crystal. This is done with the polarizer oriented at 45° with respect to the crystal axis. The birefringence causes a difference in propagation velocity along the two axis of the crystal resulting in a phase shift between the polarized components. The phase shift is determined by the birefringence of the material and its thickness. The light is recombined by a second polarizer oriented parallel or perpendicular to the first polarizer. The intensity is modulated by the phase shift as it varies from maximum for a $2n\pi$ phase shift to a minimum for a phase shift of $(2n+1)\pi$ where n is an integer and is given by

$$I = I_o \cos^2\left(\frac{\Gamma}{2}\right), \tag{1}$$

where Γ is the phase shift and at normal incidence is given by

$$\Gamma = \frac{2\pi}{\lambda}\Delta n d. \tag{2}$$

The birefringence is $\Delta n = n_e - n_o$, where n_o and n_e are the ordinary and extraordinary indices of refraction, d is the thickness, and λ is the wavelength.

The full expression for the phase shift at arbitrary angles of incidence, θ, and azimuthal angle, ϕ, is given by

$$\Gamma(\lambda,\theta,\phi) = \frac{2\pi d}{\lambda}\left\{\left[n_e^2 - \sin^2\theta\left(\cos^2\phi + \frac{n_e^2}{n_o^2}\sin^2\phi\right)\right]^{1/2} - (n_o^2 - \sin^2\phi)^{1/2}\right\}. \tag{3}$$

The birefringence, as shown by Eq. (3), has a strong azimuthal dependence to it. In a wide field version of the Lyot filter the angular dependence on θ and ϕ is significantly reduced by splitting the crystal into two parts, with each half the thickness, and orienting them such that the crystal axis are 90° apart. A half-wave retarder is oriented at 45° with respect to the crystal axis. A detailed discussion of field of view effects and advantages of wide field birefringent filters is given by Title and Rosenberg.[19]

A Lyot filter, incorporates a series of crystal stages with different thicknesses, usually in the ratio of $1:2:4:8:\ldots 2^n$, to produce a passband with a single peak and a wide free spectral range. The transmission of each stage is shown along with the total resultant spectrum in Fig. 4. In order to eliminate unwanted peaks separated by the free spectral range an interference filter is usually used.

The filter designed and utilized for NSTX has a bandwidth of 0.060 nm, with a clear aperture 75 mm, and a field of view of ±6.5°. Shown in Fig. 5 is the spectral profile of a typical filter used on NSTX.

IV. MSE-CIF DIAGNOSTIC ON NSTX

A layout of the MSE-CIF system on NSTX is shown in Fig. 6. A tangential view of the heating beam provides good spatial resolution of 2–3 cm. The collection optics is 20 cm in diameter with a 3 cm aperture in front of the optics. The collected light is imaged through a polarimeter onto a fiber optic array that is filled at $f/1.2$. The polarimeter consists of two photoelastic modulators (PEMs) oriented at 0° and 45° and followed by a polarizer at 22.5° which is the standard configuration previously used.[13,14] The fiber optic array consists of an upper and lower segment divided into 19 ferrules each. Each ferrule contains 38 fibers. The fused silica core and plastic cladding diameters are 1.0 and 1.1 mm, respectively. The two segments of ferrules are above and below the midplane with a 2 mm gap in the center containing an array of fibers for the charge exchange recombination spectros-

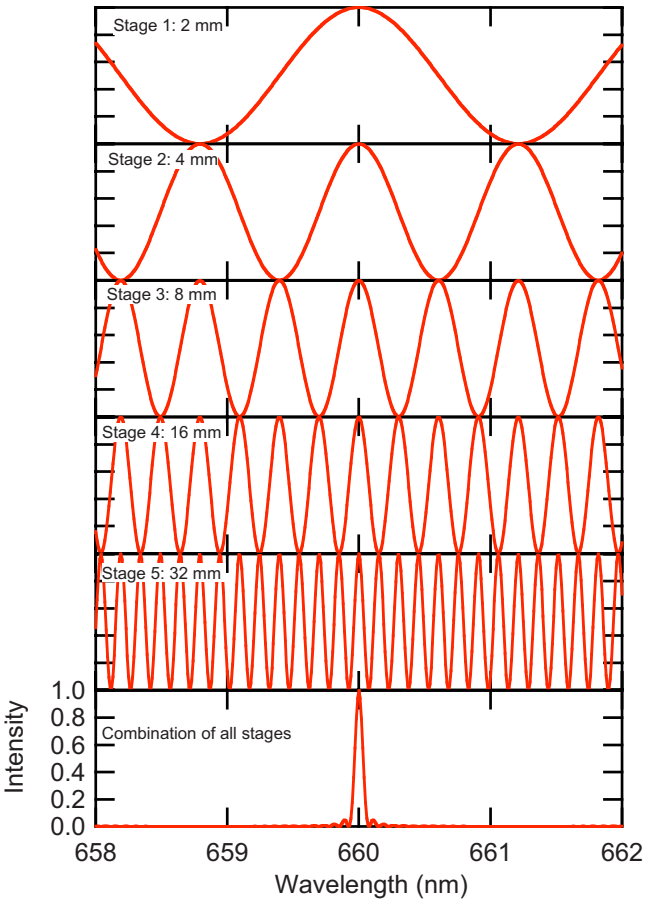

FIG. 4. (Color online) Transmission through each of five individual stages of a Lyot filter are shown. The resulting transmission is shown in the bottom panel.

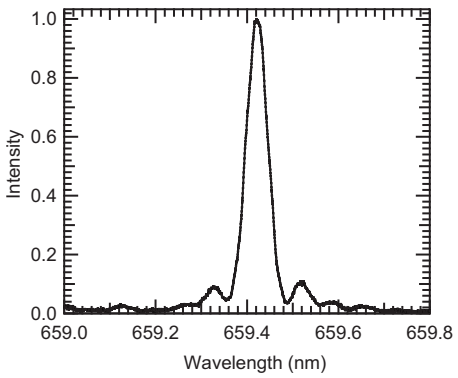

FIG. 5. The measured profile of a typical NSTX Lyot filter. The FWHM is 0.6 nm and peak transmission is 30%.

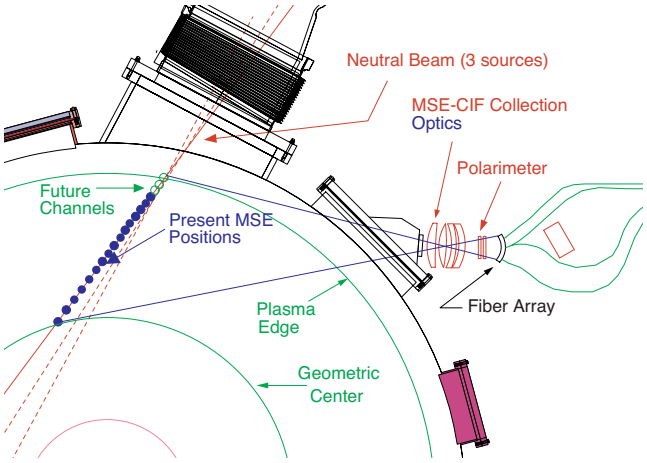

FIG. 6. (Color online) Plan view of MSE-CIF diagnostic layout on NSTX.

copy (CHERS) diagnostic. The height and width of the imaged object are 11 and 2.5 cm, respectively, on the optical axis, but varies from the inboard to outboard edge due to the variation of the magnification. The fiber optic array views from the geometric center to the outboard edge, divided into 19 spatial channels. The fiber optic bundle, which is about 14 m long, goes through a penetration in the shielding wall to a mezzanine where the filters, detectors, and data acquisition

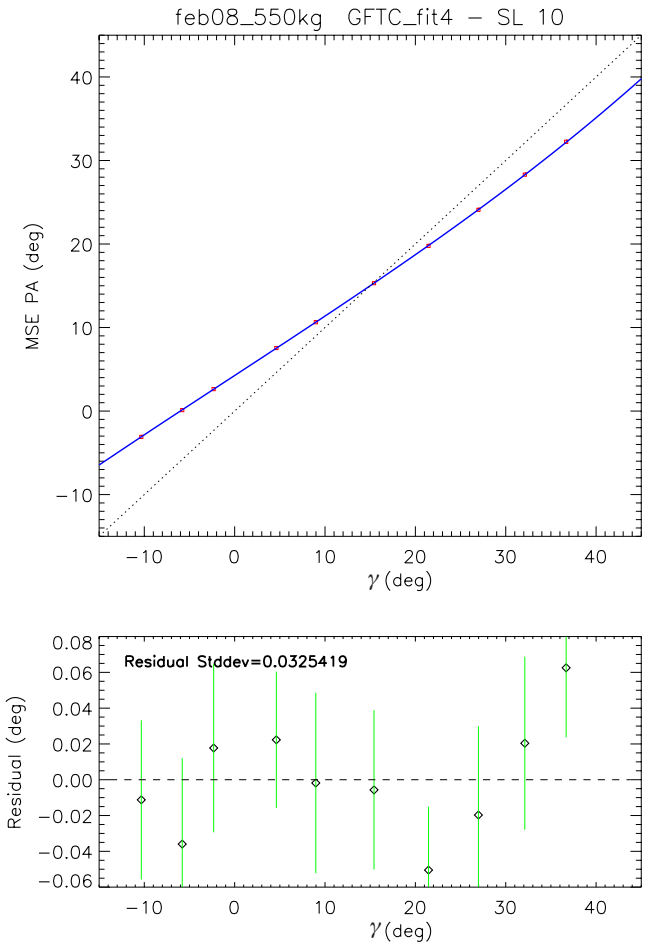

FIG. 7. (Color online) Gas filled torus calibration fit and residuals for one sight line. The y axis corresponds to the measured pitch angle before any correction, γ_{MSE}. The x axis is the actual pitch angle, γ.

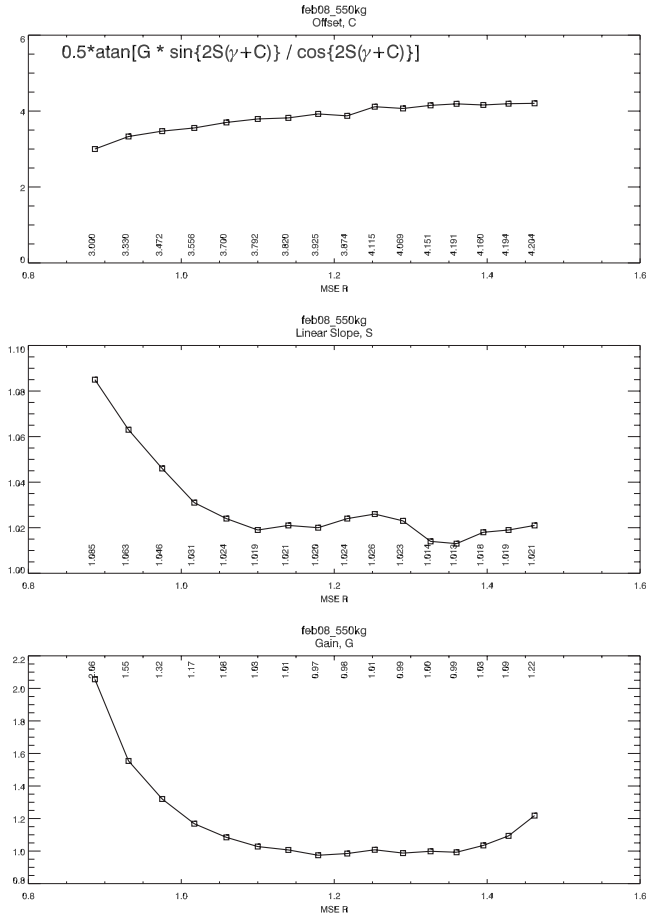

FIG. 8. The fitted parameters for all sight lines from the gas filled torus calibration.

for the diagnostic are located. The lower and upper ferrules are combined into a bundle of 76 fibers that is arranged into a 10×10 mm^2 array that is optically coupled through the filter with a collimating lens. The birefringent Lyot filter is followed by another lens to focus the light onto a 10 mm diameter avalanche photodiode (APD). The APD is cooled to 0 °C with a thermoelectric cooler and is mounted onto a printed circuit board with a high gain transimpedance amplifier. The output is then connected to an analog-to-digital module that digitizes the signal at 800 ksamples/s. This is substantially higher than the highest PEM frequency at 44 kHz. The data are analyzed using a Fourier analysis of the signal with the components at the PEM frequencies of 40 and 44 kHz used to determine the pitch angle. This is equivalent to using lock-in amplifiers as done in previous MSE systems.[14]

A very important aspect of the MSE diagnostic is calibration of the system. This has been done, as in the past,[20] using neutral beam injection into gas, without plasma, and varying the coil currents to generate known magnetic field pitch angles to calibrate with. Shown in Fig. 7 is a calibration of one of the MSE-CIF sight lines over a range of magnetic field pitch angles from nearly 40° to −10°. The y axis corresponds to the measured pitch angles, γ_{MSE} and the x axis corresponds to the input pitch angle, γ. The neutral pressure for this case is about 5×10^{-5} Torr and the neutral beam pulse length is 0.4 s. The statistical uncertainty

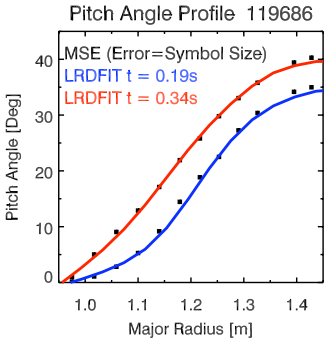

FIG. 9. (Color online) MSE-CIF data at two times and reconstruction results from LRDFIT in solid lines.

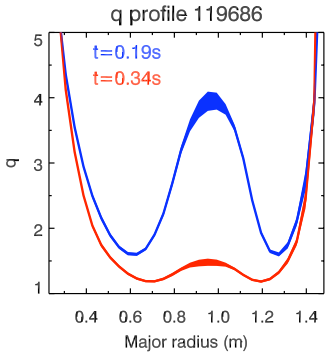

FIG. 10. (Color online) The reconstructed q profiles from LRDFIT.

is~0.1°. The model used for fitting the data is given by $\gamma_{\mathrm{MSE}}=0.5\ \tan^{-1}(G\ \sin(2S(\gamma+C)/\cos(2S(\gamma+C)))$. This includes a factor G, which is related to the viewing geometry, C is an offset due to instrumental and Faraday rotation in the optics, and S is the linear slope response of the polarimeter, and γ is the known pitch angle determined from the coil currents. The fitting parameters are determined from a least-squares fit to the data. The results for all 16 sight lines are plotted in Fig. 8. Unlike previous calibrations using beam into gas the calibration on NSTX appears not to have any offset problems in the calibration factors as described in previous work.[20] The offset problem previously encountered may be due to reneutralization of beam ions.[21] This problem could be mitigated by the large magnetic field pitch angles present in NSTX or the very narrow bandwidth filter.

In order to obtain the q profile and current density profile the MSE-CIF data have to be incorporated into an equilibrium reconstruction code to solve the Grad–Shafranov equation. This has been done using the free boundary LRDFIT equilibrium reconstruction code. The magnetic field pitch angle from the MSE-CIF diagnostic, along with the external coil currents and magnetic field and flux loop measurements, and plasma rotation are input into the code. The MSE-CIF data are corrected for the radial electric field, E_r, due to toroidal rotation and pressure gradients terms in the radial force balance shown in Eq. (6) using the CHERS data. E_r is given by the radial force balance equation,

$$E_r = \frac{1}{n_i Z_i e} \nabla P_i - v_{\theta i} B_\phi + v_{\phi i} B_\theta, \tag{4}$$

where P_i is the ion pressure, n_i is the ion number density, $Z_i e$ is the ion charge, $v_{\theta i}(v_{\phi i})$ is the poloidal(toroidal) velocity, and $B_\theta(B_\phi)$ is the poloidal (toroidal) magnetic field. The E_r correction does yet include effects from poloidal flow, which are expected to only affect the data at the edge. Shown in Fig. 9 is a reconstruction from LRDFIT of two cases of the pitch angle profile compared to the input MSE-CIF data. The data in the red plot having a flat q profile and the other example having a strongly reversed shear q profile as shown in Fig. 10. The MSE-CIF error bars are shown in the plot by the size of the symbol. The reconstruction from LRDFIT have low residuals of ~0.2°–0.3° in the plasma core, consistent with the MSE-CIF statistical uncertainties. The good fit also indicates that the MSE data are self-consistent with the magnetics and kinetic data that were incorporated used in the reconstruction. The bands on the reconstructed q profiles from LRDFIT represent the variation of the q profile by varying the input parameters into LRDFIT.

In conclusion, the MSE-CIF diagnostic on NSTX has been operating very reliably with 16 channels. The novel features of this system, the apertured optics, and wide field, narrow band Lyot filter, allow a moderately high polarization fraction with very high throughput. This has resulted in high quality data with good time resolution.

ACKNOWLEDGMENTS

This research was supported by the U.S. DOE under Grant No. DE-FG02-99ER54520 and the U.S. DOE under Contract No. DE-AC02-76CHO3073.

[1] F. M. Levinton*et al.*, Phys. Rev. Lett. **63**, 2060 (1989).
[2] F. M. Levinton, S. H. Batha, M. Yamada, and M. C. Zarnstorff, Phys. Fluids B **5**, 2554 (1993).
[3] F. M. Levinton, L. Zakharov, S. H. Batha, J. Manickam, and M. C. Zarnstorff, Phys. Rev. Lett. **72**, 2895 (1994).
[4] R. Nazikian *et al.*, Phys. Rev. Lett. **78**, 2976 (1997).
[5] Z. Chang *et al.*, Phys. Rev. Lett. **77**, 3553 (1996).
[6] M. H. Redi, R. B. White, S. H. Batha, F. M. Levinton, and D. C. McCune, Phys. Plasmas **4**, 4001 (1997).
[7] F. M. Levinton *et al.*, Phys. Rev. Lett. **75**, 4417 (1995).
[8] E. J. Strait *et al.*, Phys. Rev. Lett. **75**, 4421 (1995).
[9] E. J. Synakowski *et al.*, Phys. Rev. Lett. **78**, 2972 (1997).
[10] M. Ono *et al.*, Nucl. Fusion **40**, 557 (2000).
[11] S. M. Kaye *et al.*, Nucl. Fusion **45**, S168 (2005).
[12] E. U. Condon and G. H. Shortley, *The Theory of Atomic Spectra* (Cambridge University Press, Cambridge, 1963).
[13] F. M. Levinton, Rev. Sci. Instrum. **63**, 5157 (1992).
[14] F. M. Levinton, G. M. Gammel, R. Kaita, H. W. Kugel, and D. W. Roberts, Rev. Sci. Instrum. **61**, 2914 (1990).
[15] H. W. Kugel *et al.*, Rev. Sci. Instrum. **60**, 37 (1989).
[16] B. Lyot, Ann. Astrophys. **7**, 31 (1944).
[17] P. Connes, Rev. Opt., Theor. Instrum. **35**, 37 (1956).
[18] A. M. Title and W. J. Rosenberg, Proc. Soc. Photo-Opt. Instrum. Eng. **202**, 47 (1979).
[19] A. M. Title and W. J. Rosenberg, Appl. Opt. **18**, 3443 (1979).
[20] F. M. Levinton, S. H. Batha, and M. C. Zarnstorff, Rev. Sci. Instrum. **68**, 926 (1997).
[21] H. Yuh (unpublished).